Study of the structure, segregation, and magnetic properties of Ni-Rh clusters

Tristana Sondón,[1,2,*] Javier Guevara,[3,1] and Andrés Saúl[4]
[1]*Departamento de Física, CAC-CNEA, Avenida Gral. Paz 1499, 1650 San Martín, Argentina*
[2]*Instituto de Tecnología "Jorge Sabato," Avenida Gral. Paz 1499, 1650 San Martín, Argentina*
[3]*Escuela de Ciencia y Tecnología, Universidad de San Martín, Alem 3901, 1653 San Martín, Argentina*
[4]*Centre de Recherche en Matière Condensée et Nanosciences, CNRS, Campus de Luminy, Case 913, 13288 Marseille Cedex 9, France*
(Received 21 September 2006; revised manuscript received 23 January 2007; published 27 March 2007)

We studied the effects of size reduction and alloying on the determination of structural, segregation, and magnetic properties of 55-atom mixed Ni and Rh clusters in the whole range of concentrations. Molecular-dynamics simulations were performed to determine the cluster structures with energies and forces calculated with a semiempirical many-body potential parametrized to the alloy thermodynamic data. Magnetic properties were calculated by solving self-consistently a tight-binding Hamiltonian in the unrestricted Hartree-Fock approximation. We relate segregation behavior to magnetic properties, and we show that for low Rh concentrations there is an enhancement of the cluster magnetic moment with respect to the pure Ni one. For the central range of concentrations, we found that chemical isomers whose structures lie very close in energy present very different magnetic properties.

DOI: 10.1103/PhysRevB.75.104426 PACS number(s): 75.75.+a, 36.40.Cg, 71.20.Be

I. INTRODUCTION

Low-dimensional systems such as clusters, wires, or surfaces present, in general, different properties compared to their bulk state. In the last two decades, there has been a great amount of research on this subject due to the potential technological applications and the appearance of unexpected phenomena associated with their intermediate state between atoms and solids.

For small atomic aggregates, the variation of properties are usually caused by a combination of low-dimensional effects, which can even show oscillating values depending on their number of atoms.[1–3] All ferromagnetic bulk materials present changes on their magnetic properties in low-dimensional structures. In particular, experimental research on Ni clusters has shown enhanced magnetic moments as the cluster size decreases.[4,1]

Clusters of 4*d* transition metals (especially Pd and Rh) have gained much attention due to the possibility of presenting magnetic order. This is the case for Rh clusters, whose magnetism was first predicted theoretically[5,6] and then found experimentally by Cox *et al.*,[7] showing that Rh has very high magnetic moments per atom which decay to zero (the bulk value) for cluster sizes larger than 60 atoms. The experimental magnetic moments present oscillations as a function of size up to 40 Rh atoms; however, for those having more than 22 atoms, the measurement errors are similar to their corresponding magnetic moment values. Many theoretical works have been published on pure Ni (Ref. 8) and Rh (Ref. 9) systems using different calculation methods and approximations. Although a large number of investigations studied pure transition metal clusters, there are relatively few results on the bimetallic systems. For mixed Ni and Rh clusters, we are not aware of previous theoretical or experimental publications other than preliminary results calculated by us for very low Rh concentrations.[10]

The electronic properties of bimetallic clusters are highly dependent on their morphology, composition, and local environment of each atom in the cluster. The aim of our work is to understand the combined effects of size reduction and alloying on the magnetic properties of Ni and Rh 55-atom clusters. This size has been chosen because it is a magic number size known to be rather stable for metallic aggregates and it would give us the possibility to explore a great variety of chemical isomers as a function of the number of Rh atoms. Since we wanted to study the magnetic properties in the whole range of concentrations, we first made a systematic analysis of the structures and segregation. For this, we used molecular dynamics (MD) and Monte Carlo (MC) simulations that allowed us to identify not only the ground-state structures of 55-atom clusters at 0 K temperature but also a set of isomers lying energetically close. For these calculations, we used a potential derived from the second moment approximation (SMA) to the tight-binding method, which was parametrized to reproduce not only the pure bulk properties but also the thermodynamic properties of the alloy. The electronic and magnetic properties were calculated using a tight-binding Hamiltonian in the unrestricted Hartree-Fock approximation, parametrized to bulk materials. This method is suitable for our purpose because *ab initio* electronic structure calculations are heavy-computing methods and we need to deal with a large number of isomers.

The paper is organized as follows. Section II reports the numerical methods used in this work. In Sec. II A, we describe in detail the procedure used to find the morphology and structure of the clusters. The semiempirical potential and the simulation method used for this purpose are presented respectively in Secs. II A 1 and II A 2. The electronic structure method used to calculate cluster magnetic moments and its parametrization are described in Sec. II B 1 and the resulting bulk magnetic behavior in Sec. II B 2. We report our results and discussions of the structural and segregation properties of the bimetallic clusters in Sec. III A, and their magnetic properties are presented in Sec. III B. A summary is finally given in Sec. IV.

TABLE I. Parameters of the pure SMA potential from Ref. 19. r_0 and E_{coh} from Ref. 20. Mixed parameters were parametrized by taking into account experimental thermodynamic data.

Metal	A (eV)	ξ (eV)	p	q	r_0 (Å)	E_{coh} (eV)
Rh	0.0937	1.919	14.92	2.380	3.803	5.752
Ni	0.0952	1.554	11.34	2.270	3.523	4.435
NiRh	0.0642	1.745	13.13	2.325	3.663	

II. METHODS OF CALCULATION

A. Structure and chemical order

1. The semiempirical potential

The potential we used is derived from the SMA to the tight-binding model.[11] This semiempirical many-body potential is widely used because it reproduces rather well the thermodynamic and structural properties of most transition metals[12–18] and also because it has an analytical expression which allows a low time-consuming calculation of energies and forces. The expression of this potential has two terms: a repulsive pair contribution between ions of the Born-Mayer type and an attractive term that represents the band contribution to the bonding energy in the SMA. For a pure single-element system, the total energy can be written as

$$U_{tot} = A\sum_i \sum_{j\neq i} e^{-p[r_{ij}/r_0-1]} - \xi\sum_i \left[\sum_{j\neq i} e^{-2q[r_{ij}/r_0-1]}\right]^{1/2}, \quad (1)$$

where A, ξ, p, and q are parameters adjusted to some set of experimental data, and r_0 is the bulk interatomic distance. In this work, we used a different, more carefully tested, and improved parametrization of the SMA potential than in our previous preliminary work.[10] The recent one corrects major drawbacks both for the pure elements and the alloy (incorrect sign of the surface energy difference, incorrect outward relaxation of the surface planes, big positive mixing entalphies, etc.). The pure metal parameters are calculated in a way that reproduces exactly the interatomic distance and the cohesive energy, and approximately the bulk modulus and the elastic constants C' and C_{44} of the respective bulk materials.[19] For every atom i, the SMA expression is taken up to the second neighbor distance of the respective fcc bulk, and between the second and third neighbor distances, we use a polynomial of fifth degree in such a way that the potential and the forces go continuously to zero at the third neighbor distance and match the SMA potential expression and forces at the second neighbor one. The values of the parameters we used are reported in Table I.

Since we were interested in the properties of alloyed systems, we adjusted the mixed parameters of the SMA potential by taking into account the solution enthalpies on both extremes of the experimental phase diagram.[21] Since there is no experimental evidence of the existence of ordered phases and there exists a miscibility gap at very low temperature (below 300 K), we fitted the alloy potential parameters assuming that both enthalpies are very close to zero, which corresponds to a system that does not show a clear tendency to phase separation or to order.

The mixed p_{NiRh}, q_{NiRh}, and r_0 were taken as the arithmetic average of the ones corresponding to the pure elements, and the SMA expression, in this case, is taken up to the distance of the second neighbors of the largest size atom (Rh) and the polynomial is valid from this distance to the third neighbor distance of the smallest atom (Ni). The other two parameters (A and ξ) are shown in Table I. The resulting mixing enthalpies are $\Delta H_m = -0.015\,62$ eV/atom for Ni(Rh) and $\Delta H_m = 0.004\,87$ eV/atom for Rh(Ni), where Ni(Rh) means diluted Rh in a Ni matrix and vice versa.

We calculated the surface energies in the (100) direction by relaxing the structure of a slab of 22 planes using a quenched molecular-dynamics algorithm.[22] For this surface orientation, the values of surface energies are respectively 1633 mJ/m^2 (0.633 eV/atom) and 1943 mJ/m^2 (0.877 eV/atom) for Ni and Rh, while the experimental values are 2450 mJ/m^2 for Ni and 2700 mJ/m^2 for Rh.[23] Although the calculated surface energies are systematically smaller than the experimental ones (which is a known drawback of the SMA and similar semiempirical potentials[24–26]), the trend we get is correct. Indeed, the calculated difference between the two surface energies is 310 mJ/m^2, while the experimental one is 250 mJ/m^2.

The enthalpies of segregation to the surface ΔH_0 and to the subsurface ΔH_1 layers were calculated in both extremes of the phase diagram: diluted Rh in Ni and diluted Ni in Rh. The values obtained are shown in Table II.

Since the Rh atomic size is bigger than the Ni one, and Rh has a larger surface energy than Ni, in the Ni-rich region there is a compromise between these two competing effects that will determine the segregation behavior.[27] From Table II, it can be seen that on this region, there is a tendency to segregate Rh atoms to the subsurface layer (negative ΔH_1), which means that the most important effect in this case is the difference of surface energies. On the other hand, in the Rh-rich region, both effects will lead to a net tendency to a Ni surface segregation, as found in our calculations (negative ΔH_0).

2. Molecular dynamics

We used molecular-dynamics simulations[28,29] with the SMA potential to obtain the cluster structures. For every con-

TABLE II. Segregation enthalpies to the surface ΔH_0 and subsurface ΔH_1 layers.

	ΔH_0 (eV)	ΔH_1 (eV)
Ni(Rh)	0.108	−0.040
Rh(Ni)	−0.226	0.025

centration, the procedure we used is as follows: we took several initial high-temperature candidate structures which differ in the relative positions of Rh and Ni atoms. This gave us inequivalent chemical environments and variation of distances to the surface of the different Rh atoms present in the cluster. Afterwards, we relaxed all the structures by quenched molecular dynamics to get the structures at 0 K temperature, and from them, we selected a set of lowest-energy isomers. From a detailed study of the results for low Rh concentrations, we acquired some insight on the behavior of our potential that led us to a better guess in finding the lowest-energy candidate structures in the whole range of concentrations. Nevertheless, we also used, as an auxiliary tool, a Metropolis Monte Carlo simulation to search for possible unexpected high-temperature configurations. In every case, we confirmed that our original guesses were correct.

B. Magnetic properties

1. Tight-binding Hamiltonian

The electronic structure calculation method we used consists in solving a tight-binding Hamiltonian with a base of *spd* orbitals and intrasite electronic interaction terms following the Hubbard approximation. The site energies per orbital ϵ_{im}^0 and the hopping integrals are taken from Andersen and Jepsen's canonical linear combination of muffin-tin orbitals–atomic sphere approximation (LMTO-ASA) paramagnetic bands.[30] In this bulk parametrization, only nearest-neighbor two center parameters are considered and the dependence of these integrals on the interatomic distance r is taken through the Andersen exponent l_A as $\left(\frac{r_0}{r}\right)^{l_A}$, $l_A=l+l'+1$, where l and l' are the corresponding angular momentum quantum numbers for the corresponding orbitals, and r_0 is the experimental bulk distance.

The magnetic solutions were found by solving the Hamiltonian in the unrestricted Hartree-Fock approximation, where the site energies for the ith atom, orbital m, and spin σ are computed in the following way:

$$\epsilon_{im\sigma} = \epsilon_{im}^0 + \sum_{m'} U_{imm'} \Delta\eta_{im'} \pm \sum_{m'} \frac{J_{imm'}}{2} \mu_{im'} + \Delta\epsilon_i^{\mathrm{MAD}}, \tag{2}$$

where $\Delta\eta_{im'}$ is the difference of the electronic occupation with respect to the bulk paramagnetic values for the m' orbital, $\mu_{im'}$ is the difference of majority and minority orbital ocupations (magnetic moment contribution from this orbital) and $\Delta\epsilon_i^{\mathrm{MAD}}$ is a Madelung term. The minus and plus signs determine the energy for both spin projections. $U_{imm'}$ are the solid screened intrasite direct Coulomb integrals, whose values U_{dd} are obtained following the method of Ref. 31, using bulk occupations and keeping the U_{ss}/U_{dd} ratios the same as the atomic ones. $J_{imm'}$ are the intrasite exchange integrals and they are assumed to be zero except when m and m' are both d orbitals. J_{dd} is found, in the case of Ni, in such a way that it reproduces the experimental bulk magnetization ($\mu_{\mathrm{Ni}}=0.6\mu_B$). We used for Rh the value of $J_{dd}=0.60$ eV taken from Andersen and Jepsen,[30] who followed the method of Janak[32] on his calculation.

The Madelung term $\Delta\epsilon_i^{\mathrm{MAD}}$ consists of a sum of electrostatic potentials over all cluster sites:[33]

$$\Delta\epsilon_i^{\mathrm{MAD}} = \sum_{l\neq i} \frac{U_i}{1+U_i|\mathbf{R}_i-\mathbf{R}_l|}\Delta\eta_l, \tag{3}$$

where each term in the sum contains the interatomic electrostatic interactions between atoms on sites $\mathbf{R}_i$ and $\mathbf{R}_l$, with $\Delta\eta_l$ the total electronic occupation difference with respect to paramagnetic bulk values on the lth atom of the cluster. This expression tends to $U_i\Delta\eta_l$ for very small interatomic distances, and we have taken U_i for every element as the average value of U_{dd} and U_{sp}.[33] We verified that this election for U_i as well as the introduction of this Madelung term have very limited influence in the final results.

Transition-metal surfaces show two characteristic effects: electron spillover and d-orbital occupations almost unchanged with respect to the bulk values. It has been previously shown[33,34] that both effects can be taken properly into account by adding extra orbitals with s symmetry (s' orbitals) outside the surface. These extra s' orbitals localized in pseudo-atomic sites outside the cluster have been parametrized in order to get adequate d orbital occupations. The number of s' orbitals added is such that the coordination of each surface atom resembles, as much as possible, the bulk coordination. The energetic parameters for the tight-binding Hamiltonian are listed in Table III.

Since the diagonal terms depend on the orbital ocuppations for every spin, the Hamiltonian was solved self-consistently by diagonalizing at each step the spin-up and spin-down matrices until a charge convergence of less than 10^{-4} electrons was obtained. We verified that this charge convergence always leads to a magnetic moment error of the order of $10^{-3}\mu_B$. In order to define the Fermi level, states were considered degenerate if their energies lie within 0.010 eV or less, independent of their spin. These degenerate states are then assumed to be equally filled, leading sometimes to a fractional filling of the highest occupied states, but we required an integer total magnetic moment for our cluster calculations.

2. Bulk calculation

In order to identify and isolate the main properties of clusters, we calculated the bulk magnetic behavior with our tight-binding Hamiltonian in the whole range of compositions using a cubic 32-atom periodic cell with dimensions proportional to the Rh concentration.

In the first place, we have calculated the pure bulk Ni and Rh systems at their experimental lattice parameters. The magnetic moments obtained were $\mu_{\mathrm{Ni}}=0.6\mu_B$ and $\mu_{\mathrm{Rh}}=0\mu_B$. In Fig. 1(a), we show the total up and down densities of states of Ni bulk, and in Fig. 1(b) the ones corresponding to Rh bulk. Both densities of states (DOSs) are in good agreement with *ab initio* calculations by Moruzzi *et al.*[35]

We next calculated a 32-atom Ni cell with a Rh impurity, obtaining a magnetic moment for this atom of $0.81\mu_B$. This is an interesting result, which shows that Rh atom gets highly polarized in a Ni environment. The total charge transfer from Ni to the Rh impurity is rather small (0.08 electrons), al-

TABLE III. Tight-binding parameters used in this work were taken from Refs. 30 and 31. All the parameters are in eV, except for the dimensionless l_A. The two site integrals are listed from the second to the fourth column. In the fifth column, we show the Andersen exponent l_A used to calculate the dependence of these integrals on the interatomic distance (see text). ϵ_m is the site energy of the m orbital, $U_{mm'}$ are the intrasite direct Coulomb integrals between orbitals m and m', and J_{dd} is the exchange integral among d orbitals.

	Ni	Rh	Ni-Rh	l_A		Ni	Rh
$ss\sigma$	−1.064	−0.966	−1.014	1	ϵ_s	1.663	1.861
$pp\sigma$	1.878	1.504	1.681	3	ϵ_p	6.646	5.923
$pp\pi$	−0.235	−0.188	−0.210	3	ϵ_{e_g}	−3.018	−2.957
$dd\sigma$	−0.555	−0.999	−0.745	5	$\epsilon_{t_{2g}}$	−3.135	−3.167
$dd\pi$	0.237	0.427	0.318	5	$\epsilon_{s'}$	5.012	5.012
$dd\delta$	−0.022	−0.039	−0.029	5	U_{ss}	1.00	0.95
$sp\sigma$	1.408	1.200	1.300	2	U_{sd}	1.20	1.05
$sd\sigma$	−0.739	−0.945	−0.836	3	U_{dd}	2.73	2.63
$pd\sigma$	−0.998	−1.199	−1.094	4	J_{dd}	1.07	0.60
$pd\pi$	0.238	0.285	0.260	4			

though Rh d orbitals lose 0.068 electrons. Even when this charge transfer is very small, the hybridization of the Rh bands with Ni states produces a d band splitting on rhodium, leading to a high polarization. This can be seen in Fig. 2, where we show the projected densities of states of the Rh impurity. The hybridization between the Ni and Rh bands produces peaks in the DOS near the Fermi level and at the bottom of the bands (between −5 and −4 eV). Not only the Rh magnetic moment is increased, but also the average Ni moments get slightly enhanced.

To compare our method with experimental values, we calculated the bulk alloy magnetic behavior for all Rh concentrations. In Fig. 3(a), we show the average experimental Ni and Rh magnetic moments from Ref. 36, and in Fig. 3(b) the calculated ones. As shown in this figure, our tight-binding calculation leads systematically to lower magnetic moments, but it follows a similar overall behavior as the experimental one. At low Rh concentrations, both experimental and calculated Rh magnetic moments are larger than the Ni ones up to around 10% Rh. It is worth noting that our calculations led to negligible magnetic moments at approximately 25% Rh, while the experimental results show zero magnetization for concentrations higher than 35% Rh.

It can be seen in Fig. 3 that the experimental Rh magnetic moment interpolated to a concentration equivalent to one Rh impurity in a 32-atom cell (3.12% Rh) is approximately $1.4\mu_B$, while we have obtained $0.81\mu_B$. Attempting to reproduce this value, we made a set of calculations by changing the J_{dd}^{Rh} parameter, with the constraint of keeping a nonmagnetic Rh bulk. Following the Stoner criterion, J_{dd}^{Rh} must be smaller than 1.2 eV in order to satisfy this constraint. Our

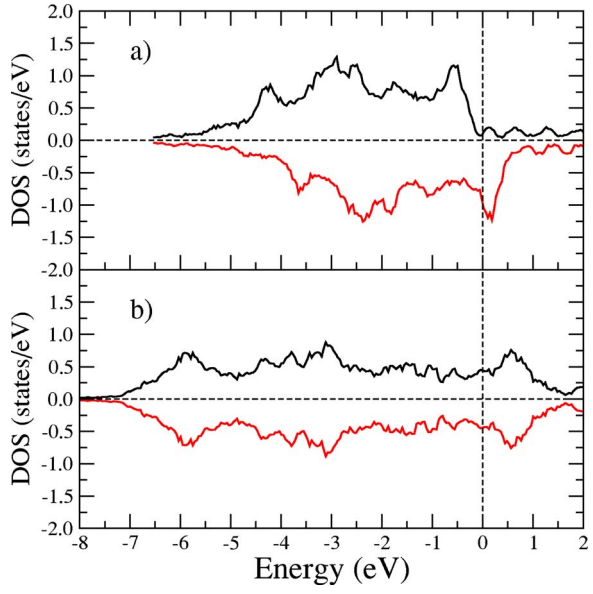

FIG. 1. (Color online) Total up and down densities of states per atom calculated with our tight-binding Hamiltonian for bulk metals. (a) The self-consistent solution leads to ferromagnetism in Ni, and (b) Rh bulk remains without magnetic order.

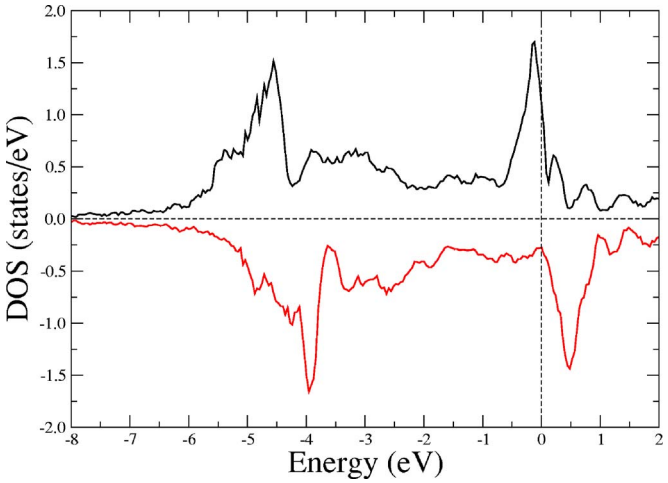

FIG. 2. (Color online) Projected total density of states of the Rh atom calculated as an impurity in a Ni cell. The polarization obtained is the effect of the hybridization between Ni and Rh states.

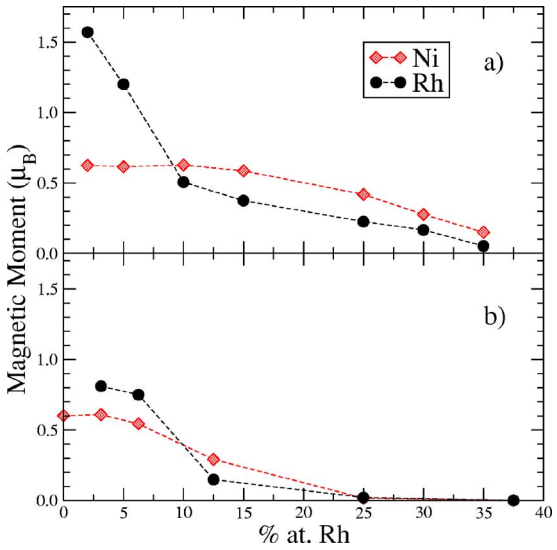

FIG. 3. (Color online) (a) Experimental (Ref. 36) and (b) calculated bulk magnetic moments (in μ_B/atom) as a function of Rh concentration. We show in both cases the average per atom, Ni and Rh magnetic moments.

results obtained for this J_{dd}^{Rh} are $\mu_{Total}=0.620\mu_B$, $\mu_{\mathrm{Ni}}=0.594\mu_B$, and $\mu_{\mathrm{Rh}}=1.407\mu_B$. It is then necessary to double the J_{dd}^{Rh} parameter in order to obtain the experimental Rh magnetic moment. However, we found that using it to compute the magnetism in the whole range of Rh concentrations leads to very high magnetic moments in contradiction to the experimental trends. Since there is no physical basis to introduce such a high exchange parameter for a nonmagnetic atom (which would be even higher than the Ni one and similar to the usual one for Co) and the obtained magnetic properties are far from the experimental ones, we continued to use the original exchange parameter for Rh (which is, after all, a result of an *ab initio* calculation).

III. RESULTS

A. Structure of Ni-Rh clusters

We found by using our MD and MC simulations that, in all cases, the minimum energy structures of the 55-atom clusters are icosahedral. For pure Rh clusters, other works confirm that the icosahedral structure is the most stable one: *ab initio* calculations[38] show that for different cluster sizes, several stable structures such as cuboctahedral, decahedral, or icosahedral are possible, but, in particular for 55-atom clusters, the icosahedral structure is the one which presents the lowest energy. Barreteau *et al.*[39] also performed tight-binding calculations, showing that the icosahedral structure is energetically favorable for a 55-atom Rh cluster.

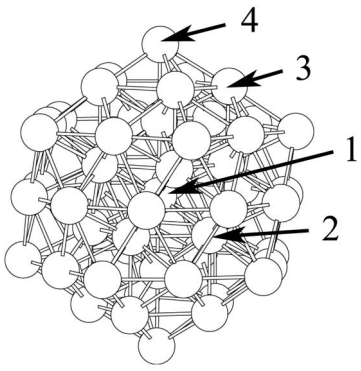

FIG. 4. Icosahedral 55-atom cluster showing the four inequivalent sites: (p1) center, (p2) subsurface layer, (p3) moderate coordinated surface sites, and (p4) low coordinated surface sites.

For a monoatomic system, the icosahedral geometry of this cluster has four inequivalent positions, which correspond to the single atom at the center of the cluster (p1), 12 atoms in the second shell, which is also the subsurface layer (p2), 30 atoms in moderate coordinated sites at the surface (p3), and 12 atoms in the low coordinated sites at the surface (p4) (see Fig. 4).

1. Low Rh concentration

The energies and chemical configurations of the obtained icosahedral $Ni_{55-x}Rh_x$ clusters at low Rh concentration are shown in Table IV. For $x=1$, we find that the lowest-energy structure is the one which has the Rh atom at the moderate coordinated surface position (p3). The next configuration in

TABLE IV. Energies of different chemical configurations for mixed $Ni_{55-x}Rh_x$ clusters with $x=1$, 2, and 3. The numbers l, m, and n in the first, third, and fifth columns represent the position of the Rh atoms in the four inequivalent sites of the 55-atom icosahedral cluster (see Fig. 4). The zero of energy corresponds to the lowest-energy configuration for each Rh concentration.

$Ni_{54}Rh_1$		$Ni_{53}Rh_2$		$Ni_{52}Rh_3$	
l	E_l (eV)	lm	E_{lm} (eV)	l_{mn}	E_{lmn} (eV)
3	0.000	33	0.000	333	0.000
2	0.078	23	0.075	233	0.105
4	0.292	22	0.162	232	0.170
1	0.973	34	0.292	222	0.275
		44	0.572	334	0.340
		12	1.120	443	0.584
		14	1.244	…	
		…		…	

TABLE V. Difference in energy between the structures with one Rh atom at the surface and at the subsurface layer, for clusters of two different geometries (icosahedral and fcc) and sizes. To compare with bulk, we also show the result for a semi-infinite system with a (100) surface. We see that the only case in which there is a Rh segregation to the surface is for the 55-atom icosahedral cluster.

	55	147	309	561	∞
Icoshaedral	−0.078	0.010	0.071	0.090	
fcc	0.028	0.097	0.121	0.135	
Slab(100)					0.148

energy has the Rh atom at the subsurface layer (p2), while the highest energy corresponds to the Rh atom at the center position (p1).

The icosahedral 55-atom cluster has such a particular topology that in pure clusters the central atom is under a compressive tension, which is high enough to give rise to negative vacancy-formation energies.[15] In our system, there is a size difference of +8% between Rh and Ni atoms, therefore the placement of a Rh atom at the central position of the cluster is strongly energetically penalized with ≈1 eV difference with respect to the lowest-energy structure, as can be seen in the second column of Table IV. For the lowest-energy structure, we see that the Rh is placed at a surface position, instead of at the subsurface layer as in semi-infinite systems (see Table II). This is a direct consequence of the icosahedral topology and the size of the cluster, because in the 55-atom icosahedral cluster, the second shell (p2) is also under compression, and placing Rh atoms on it would lead to a rise in energy caused by the high stress. To support this, we calculated the structures and energies of icosahedral and fcc (cuboctahedral) clusters of several sizes, having one Rh atom at the surface or at the subsurface shell. As can be seen in Table V a change in the cluster geometry (from icosahedral to fcc) or an increment in size for icosahedral clusters produces the lowest-energy structures to be the ones with the Rh atom at the subsurface layer (p2). This is due to the fact that for these structures, the stress asocciated with that shell is lower than for the 55-atom cluster, and also, as the size of the cluster grows, we approach the bulk behavior.

2. Higher Rh concentrations

In this case, Rh atoms can be placed either at different shells (inequivalent positions p1–p4) or at different positions in a given shell. In both cases, they can also differ in their proximity. If we change the position of one Rh atom inside a shell, the highest total energy difference that can be obtained is 0.03 eV. The lowest-energy structure is always the one which presents the Rh atom far away from each other. The change in position to another shell yields a higher variation in energy. Therefore, for structures with two and three Rh atoms ($x=2$ and 3), the values shown in the Table IV correspond to the average energy difference of configurations having each Rh atom in a given shell. For example, for $x=2$ ($x=3$) the configuration with $lm=33$ ($lmn=333$) means that all the Rh atoms are in p3. These are the lowest-energy structures. The next set of isomers corresponds to moving one atom from the surface to the subsurface position (configuration 23 for $x=2$ and configuration 233 for $x=3$). It is interesting to note that the configurations of higher energies that we obtain with our semiempirical many-body potential, listed in Table IV can be predicted from the solutions for $x=1$, i.e., $E_{lm} \simeq E_l + E_m$ and $E_{lmn} \simeq E_l + E_m + E_n$.

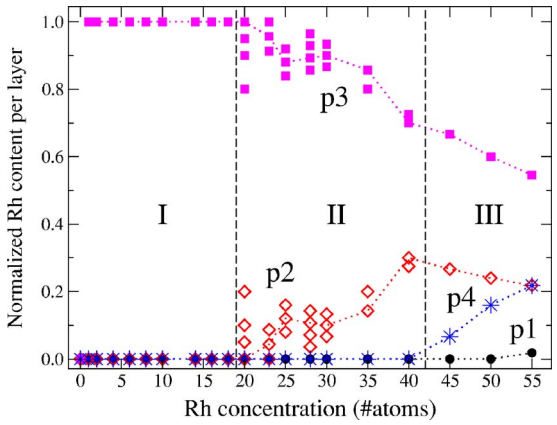

FIG. 5. (Color online) Fraction of Rh atoms in nonequivalent positions (p1–p4) as a function of the total number of Rh atoms in the cluster, for all sets of low-energy isomers. The corresponding values to the minimum energy structures are connected by dotted lines.

3. Complete range of Rh concentrations

To discuss the main trends on segregation, we show in Fig. 5 the normalized concentration of Rh atoms for each type of nonequivalent positions as a function of the total number of Rh atoms in every cluster. Here we consider for each concentration the lowest-energy structure and all the isomers lying within a range of 0.05 eV.

Our results show that there are three well-defined segregation zones. The two main effects that determine this behavior are the difference of surface energies and of atomic sizes. As we discussed in Sec. II A 1, the first effect will favor Ni atoms to be at surface positions, while the second will favor Rh segregation. For zone I (Rh concentrations below 20 atoms, 36 at. % Rh), these isomers present all their Rh atoms on the type 3 positions, indicating that up to this concentration, the atomic size difference is the leading effect. In zone II (from 20 to 40 Rh atoms), there are several isomers that are close in energy, having some of their Rh atoms in the type 2 positions. This means that not all the 30 available positions of type 3 are filled before adding atoms to the subsurface layer (p2). Therefore, in this zone, there is a competition between the differences of surface energies and atomic sizes of the atoms that determines the segregation behavior. For zone III (higher Rh concentrations), the lowest coordination positions (p4) begin to get occupied up to the 54-atom Rh cluster, in which the Ni atom is at the central position. In agreement with the results discused earlier about the stress present on inner shells of these clusters, for very low Ni concentration, one of the Ni atoms is always placed at the center of the cluster even when the properties of the

TABLE VI. Magnetic moments for pure icosahedral and fcc (cuboctahedral) clusters. In the first column, we show the average of the total magnetic moment per atom. In the next four ones, we show the average magnetic moments for layers of inequivalent atoms (see text). In the last column, we show the total magnetic moment corresponding to the sum of the 147 s' orbitals.

	Magnetic moment ($\mu_B/at.$)					
	Total	$p1$	$p2$	$p3$	$p4$	μ_{tot} (μ_B) s'
Ni_{55}^{ico}	0.727	0.689	0.934	0.669	0.724	–0.711
Rl_{55}^{ico}	0.000	0.000	0.000	0.000	0.000	0.000
Ni_{55}^{fcc}	0.727	0.697	0.808	0.686	0.782	–0.357
Rh_{55}^{fcc}	0.357	–0.013	0.252	0.318	0.582	0.102

bulk alloyed system would give a tendency to segregate Ni to the surface (see Table II). Nevertheless, it is clear that, in our case, the system lowers its energy by placing the smallest atom at the most stressed position of the 55-atom cluster, the central one.

B. Magnetic moments of Ni-Rh clusters

We have calculated the magnetic properties of icosahedral clusters following the method described in Sec. II B 1. For the sake of comparison, we also show results on fcc (cuboctahedral) clusters relaxed by MD. We first show the results obtained for pure icosahedral and fcc clusters. We next analyze the effect of introducing a Rh impurity on pure Ni clusters at different positions. Finally, we show the magnetic behavior of icosahedral clusters in the whole range of concentrations. In our calculations, we tested ferro- and antiferromagnetically aligned solutions, finding in all cases that the ferromagnetic ones had lower energies, and therefore, our results always refer to spins with a parallel orientation.

1. Pure clusters

We have previously described the icosahedral cluster geometry, where from the center to the lowest coordinated atoms at the surface, the number of inequivalent positions are (1, 12, 30, 12). For the cuboctahedral clusters we have (1, 12, 6, 24, 12), and to compare both geometries, we present the results for fcc clusters as we did for the icosahedral ones, where the (p1)–(p4) positions have similar meanings: (p1) is the central position, (p2) the subsurface layer, (p4) are the lowest coordinated positions at the surface, and the rest of the atoms at the surface are taken at position 3, even when they are not exactly equivalent, having in this way the same number of atoms per layer.

In Table VI, we show the magnetic moments of pure Ni and Rh 55-atom icosahedral and fcc clusters. We used 147 s' orbitals in all cases and we show their total magnetic contribution. The maximum magnetic moment per s' orbital is thus equal to $0.0048\mu_B$ for the icosahedral Ni_{55} cluster, and lower for the rest of the calculated clusters. We found that the Ni clusters have an enhanced total magnetic moment ($0.727\mu_B$) with respect to the calculated and experimental bulk value ($0.6\mu_B$). The total magnetic moments on both types of clusters are the same, but not the moments per layer due to their difference in geometry, which introduces changes in their interatomic distances (the icosahedral cluster is more compact than the cuboctahedral one). For the pure Rh icosahedral cluster, we found no magnetic order, while for the fcc cluster, there is a polarization on the surface and subsurface layers as a consequence of its geometry. Our results are in very good agreement with calculations presented in Ref. 37, where the authors show a nonmagnetic Rh 55-atom icosahedral cluster and a magnetic cuboctahedral one, claiming that their magnetic moments are in accordance with local spin-density approximation *ab initio* calculations.

2. Low Rh concentration

We have introduced a Rh impurity in icosahedral and fcc Ni clusters. The results obtained for all the possible inequivalent sites occupied by the impurity are shown in Table VII. It is interesting to note that in all cases there is an enhancement of the total magnetic moments with respect to pure Ni clusters. This is the result of the hybridization between Ni and Rh orbitals (as we have obtained for our bulk calculations), along with surface effects which produce a great enhancement on Rh magnetic moments. For both geometries, the general trend is the same: the Rh magnetic moments are increased when their total coordination (the total number of nearest neighbors) is decreased [from positions (p1) to (p4)] and the average Ni magnetic moments are slightly reduced. When a Rh atom is placed at the central position in the fcc cluster, we found that it behaves very much as an impurity in bulk, since its magnetic moment is very close to the Rh impurity value in Ni bulk, as was discussed in Sec. II B 2.

3. Complete range of Rh concentrations

So far, we have described the magnetism on pure Rh cluster and one Rh impurity cluster. Now we will analyze the effect of the presence of several Rh atoms on the clusters. When we made the study of structural isomers, the presence of Rh atoms in the same layer [(p1)–(p4)] did not have a big influence on segregation properties, since the energy of these configurations were very close. On the contrary, the magnetic properties are highly dependent on the relative proximity of the Rh atoms. In this case, we need more information on the total coordination of the Rh atoms; we also need to know how many are nearest neighbors of each other, since this

TABLE VII. Calculated magnetic moments of Ni icosahedral and fcc clusters with one Rh impurity for all Rh inequivalent positions (p1–p4). The sum of all the magnetic moments of the 147 s' orbitals are also shown. The magnetic moments are expressed in Bohr magnetons (μB).

		$\mu_{tot}/at.$	$\mu_{Ni}/at.$	$\mu_{Rh}/at.$	$\mu_{s'}$
ico	Ni_{55}	0.727	0.740	—	−0.711
	$Ni_{54}Rh(p1)$	0.745	0.762	0.558	−0.692
	$Ni_{54}Rh(p2)$	0.745	0.747	1.286	−0.607
	$Ni_{54}Rh(p3)$	0.745	0.745	1.452	−0.697
	$Ni_{54}Rh(p4)$	0.745	0.741	1.548	−0.555
	Rh_{55}	0.000	—	0.000	0.000
fcc	Ni_{55}	0.727	0.734	—	−0.357
	$Ni_{54}Rh(p1)$	0.745	0.752	0.799	−0.387
	$Ni_{54}Rh(p2)$	0.745	0.742	1.235	−0.289
	$Ni_{54}Rh(p3)$	0.745	0.738	1.419	−0.294
	$Ni_{54}Rh(p4)$	0.745	0.734	1.686	−0.349
	Rh_{55}	0.357		0.356	0.102

determines the effect of hybridization with Ni orbitals on their magnetic moments. A magnitude that will quickly reflect this effect is the partial Rh-Rh coordination, defined as the average, over all the Rh atoms in the cluster, of the number of Rh first neighbors that they have. The Rh-Ni coordination has an analog definition.

From pure Ni to pure Rh clusters, we then expect to obtain a magnetic behavior that will be a combination of two effects: (1) the Rh polarization due to hybridization with Ni orbitals (that increases the Rh magnetic moment from zero to around $0.8\mu_B$ in bulk) and (2) the enhancement of the Rh magnetic moments due to the proximity of these atoms to the surface (which can increase to even twice its bulk impurity value when a Rh atom at p4 is completely surrounded by Ni atoms). The first effect can be easily analyzed as a funcion of the partial Rh-Rh coordination, and the second one, by computing the average of the total coordination of Rh atoms.

We present in Fig. 6(a) the average of the total Ni and Rh magnetic moments per atom as a function of Rh concentration for the lowest-energy icosahedral clusters and their chemical isomers, whose structures were discussed in Sec. III A. In Fig. 6(b), we show the average Rh-Rh, Rh-Ni, and total coordinations of Rh atoms for the mentioned cluster structures.

The first important general result we found is that the range of magnetic order for clusters was extended with respect to bulk behavior from 25% Rh to 73% Rh. We also note a strong correspondence between the magnetic and segregation behaviors, and therefore, we will describe in detail the results for every zone of the diagram.

The main characteristic of the whole zone I is that for all clusters, we found enhanced total magnetic moments with respect to pure Ni bulk. In particular, we show that for Rh concentrations lower than 10 Rh atoms (18.8% Rh), the total magnetic moments are even higher than for the pure Ni cluster. The interesting enhancement property of this zone is related to the surface positioning (p3) of the Rh atoms and to the fact that the partial Rh-Rh coordinations remain low, which means that the Rh atoms are mainly surrounded by Ni. The high magnetic moments obtained are therefore a product of surface effects.

For zone II (central interval of concentrations), we obtained an important dispersion in the magnetic moments for different isomers of the same composition. This variation is

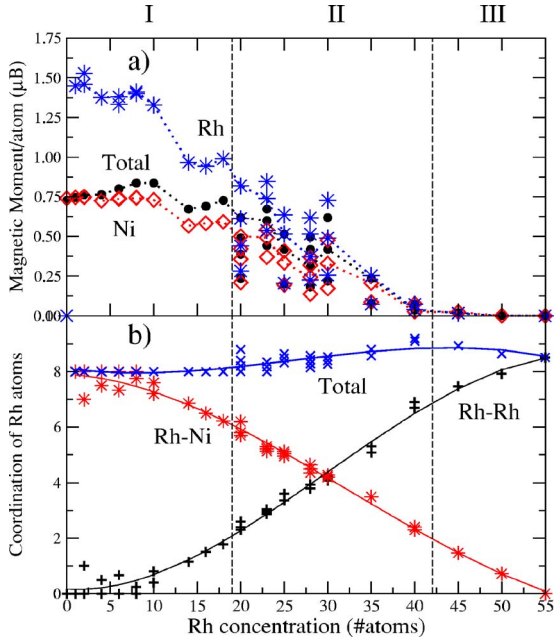

FIG. 6. (Color online) (a) Average of the total Ni and Rh magnetic moments for icosahedral clusters. We show for every composition the results for the lowest-energy set of isomers. In (b), we show the average Rh-Rh, Rh-Ni, and total coordinations for Rh atoms. Both graphs are divided in three zones, which correspond to the different segregation behaviors presented in Fig. 5 In (a), the dotted lines connect the moments of the lowest-energy structures, and in (b), the lines are only a guide for the eyes.

due to the different atomic environments for the Rh atoms, which present changes in their Rh-Rh and total coordinations, as is clearly shown in Fig. 6(b). It is in this range of concentrations where the interplay of surface and hybridization effects determines the magnetic behavior of these set of isomers.

Finally, in zone III, for concentrations higher than 42 Rh atoms (~76% Rh), high Rh-Rh coordination produces very low magnetic moments, reaching a null value at the concentration of 100% Rh. In particular, for one Ni atom the lowest-energy structure has the impurity atom at the central position. In this case, the Ni magnetic moment is zero and even if this atom is placed at the surface, it presents magnetic moments below $0.06\mu_B$.

It is interesting to note that the Ni-Rh system presents, in some sense, a similar behavior to the Co-Rh one. In a previous work,[40] we showed that there is an enhancement of the total magnetic moment with respect to the alloy values. This result also agrees with experimental measurements[41] and other theoretical works on that system.[42]

Following the analysis made earlier with respect to the segregation behavior, since Ni and Co have almost the same size and the surface energy difference of Co and Rh is lower than for the Ni-Rh system, we can predict that the compromise between both effects will give, in the case of the Co-Rh system, a Rh segregation to the surface in bulk and an extended zone I for cluster results.

IV. SUMMARY

We studied the role played by size reduction and alloying effects on structural, segregation, and magnetic properties of mixed Ni and Rh 55-atom clusters.

Molecular-dynamics simulations using the SMA potential allowed us to study in detail the lowest-energy set of isomers for mixed clusters on the whole range of Rh concentrations, obtaining that in all cases the icosahedral structure was energetically favored. We found that the geometry and size of the clusters have a big influence on the Rh surface segregation and that even though the mixing enthalpy for the system is close to zero, we obtain an "effective" order on this system.

The two main driving forces which determine segregation behavior of the clusters, the surface energy and atomic size difference of both metals, define three different zones as a function of Rh concentrations, depending on the balance of these competing effects. An interesting result is that, for the central zone of concentrations, we found a great number of isomers lying in a small range of energies around the lowest-energy structures, but even if they are similar from the structural point of view, their magnetic properties turned out to be very different.

For pure icosahedral and cuboctahedral Ni clusters, we found that the size reduction effect enhances their magnetic moments, while for pure Rh, this produces a small magnetic moment on the fcc cluster but none in the icosahedral one. When we introduce a Rh impurity in a pure Ni cluster, its contribution to the cluster magnetism (which is highly dependent on its position in the cluster) always leads to an enhancement of the total magnetic moment. Compared to our bulk calculations, Rh magnetic moments can even get enhanced by a factor of around 2.

We found that the critical concentration at which the magnetic ordering is lost is extended from 25% Rh for the alloy to almost 76% Rh for 55-atom clusters. For low Rh concentrations, there is an enhancement of the total magnetic moments mainly due to surface effects. In the central zone of concentrations, the resulting magnetic moments are a combination of hybridization and size reduction effects, and we have shown how these moments are directly related to the total and Rh-Rh coordinations for the set of lowest-energy isomers. For concentrations above 76% Rh, the Ni-Rh coordinations are so low that it leads to negligible total magnetic moments for the clusters.

ACKNOWLEDGMENTS

We acknowledge PICT 03-10698 and Proyecto IM40, both of Agencia Nacional de Promoción Científica y Tecnológica, and PIP 6016 of CONICET for partial support. We also acknowledge ECOS-SECyT through Grant No. A03E06 and CNRS through the Projet International de Coopération Scientifique (PICS) program, and the Université de la Mediterranée for travel support. J.G. and T.S acknowledge support from CONICET. We want to thank Christine Mottet, Guy Treglia, and Christophe Bichara for useful discussions.

*Electronic address: sondon@tandar.cnea.gov.ar

[1] S. E. Apsel, J. W. Emmert, J. Deng, and L. A. Bloomfield, Phys. Rev. Lett. **76**, 1441 (1996).
[2] M. B. Knickelbein, J. Chem. Phys. **116**, 9703 (2002).
[3] Shu-Rong Liu, Hua-Jin Zhai, and Lai-Sheng Wang, Phys. Rev. B **65**, 113401 (2002).
[4] I. M. L. Billas, A. Châtelain, and W. A. de Heer, Science **265**, 1682 (1994).
[5] R. Galicia, Rev. Mex. Fis. **32**, 51 (1985).
[6] B. V. Reddy, S. N. Khanna, and B. I. Dunlap, Phys. Rev. Lett. **70**, 3323 (1993).
[7] A. J. Cox, J. G. Louderback, and L. A. Bloomfield, Phys. Rev. Lett. **71**, 923 (1993); A. J. Cox, J. G. Louderback, S. E. Apsel, and L. A. Bloomfield, Phys. Rev. B **49**, 12295 (1994).
[8] N. Fujima and T. Yamaguchi, Phys. Rev. B **54**, 26 (1996); F. Aguilera-Granja, S. Bouarab, M. J. Lopez, A. Vega, J. M. Montejano-Carrizales, M. P. Iniguez, and J. A. Alonso, *ibid.* **57**, 12469 (1998); Xiangang Wan, Lei Zhou, Jinming Dong, T. K. Lee, and Ding-sheng Wang, *ibid.* **69**, 174414 (2004); G. M. Pastor, J. Dorantes-Davila, and K. H. Bennemann, *ibid.* **70**, 064420 (2004); Antonis N. Andriotis and Madhu Menon, Phys. Rev. Lett. **93**, 026402 (2004).
[9] Yang Jinlong, F. Toigo, and Wang Kelin, Phys. Rev. B **50**, 7915 (1994); Zhi-Qiang Li, K. Ohno, and Y. Kawazoe, J. Phys.: Con-

dens. Matter **7**, 47 (1995), **7**, 7367 (1995); Brigitte Piveteau, Marie-Catherine Desjonqueres, Andrzej M. Oles, and Daniel Spanjaard, Phys. Rev. B **53**, 9251 (1996); P. Villasenor-Gonzalez, J. Dorantes-Davila, H. Dreysse, and G. M. Pastor, *ibid.* **55**, 15084 (1997); R. Guirado-Lopez, D. Spanjaard, and M. C. Desjonqueres, *ibid.* **57**, 6305 (1998); Chang-Hong Chien, Estela Blaisten-Barojas, and Mark R. Pederson, Phys. Rev. A **58**, 2196 (1998); B. V. Reddy, S. K. Nayak, S. N. Khanna, B. K. Rao, and P. Jena, Phys. Rev. B **59**, 5214 (1999); C. Barreteau, R. Guirado-Lopez, D. Spanjaard, M. C. Desjonqueres, and Andrzej M. Oles, *ibid.* **61**, 7781 (2000); R. Guirado-Lopez, M. C. Desjonqueres, and D. Spanjaard, *ibid.* **62**, 13188 (2000); F. Aguilera-Granja, J. L. Rodriguez-Lopez, K. Michaelian, E. O. Berlanga-Ramirez, and A. Vega, *ibid.* **66**, 224410 (2002); Yuannan Xie and J. A. Blackman, Phys. Status Solidi A **189**, 763 (2002).

[10] T. Sondón and J. Guevara, Physica B **354**, 303 (2004).

[11] V. Rosato, M. Guillopé, and B. Legrand, Philos. Mag. A **59**, 321 (1989).

[12] M. Guillopé and B. Legrand, Surf. Sci. **215**, 577 (1989).

[13] R. Ferrando and G. Tréglia, Phys. Rev. B **50**, 12 104 (1994).

[14] A. Khoutami, B. Legrand, C. Mottet, and G. Tréglia, Surf. Sci. **307**, 735 (1994).

[15] C. Mottet, G. Tréglia, and B. Legrand, Surf. Sci. Lett. **383**, L719 (1997).

[16] F. Montalenti and R. Ferrando, Phys. Rev. B **59**, 5881 (1999); Phys. Rev. Lett. **82**, 1498 (1999).

[17] F. Baletto, C. Mottet, and R. Ferrando, Surf. Sci. **446**, 31 (2000); Phys. Rev. Lett. **84**, 5544 (2000).

[18] F. Baletto, R. Ferrando, A. Fortunelli, F. Montalenti, and C. Mottet, J. Chem. Phys. **116**, 3856 (2002).

[19] Isabelle Meunier, Ph.D. thesis, Université de la Mediterranée, 2001; Stéphane Olivier, Ph.D. thesis, Université de la Mediterranée, 2004.

[20] C. Kittel,*Introduction to Solid State Physics* (Wiley, New York, 2004).

[21] P. Nash,*Phase Diagrams of Binary Nickel Alloys* (ASM International, Metals Park, OH, 1991).

[22] B. Legrand, G. Tréglia, M. C. Desjonqueres, and D. Spanjaard, J. Phys. C **19**, 4463 (1986).

[23] F. R. De Boer, R. Boom, W. C. N. Mattens, A. R. Miedema, and A. K. Nielssen, *Cohesion and Structure* (North-Holland, Amsterdam, 1988).

[24] S. M. Foiles, M. I. Baskes, and M. S. Daw, Phys. Rev. B **33**, 7983 (1986).

[25] M. S. Stave, D. E. Sanders, T. J. Raeker, and A. E. DePristo, J. Chem. Phys. **93**, 4413 (1990).

[26] J. Guevara, A. M. Llois, and M. Weissmann, Phys. Rev. B **52**, 11509 (1995).

[27] A. Saúl, B. Legrand, and G. Tréglia, Phys. Rev. B **50**, 1912 (1994).

[28] D. Frenkel and B. Smit, *Understanding Computer Simulations: From Algorithms to Applications* (Academic, New York, 2004).

[29] M. P. Allen and D. J. Tildesley, *Computer Simulation of Liquids* (Oxford University Press, New York, 1987).

[30] O. K. Andersen and O. Jepsen, Phys. Rev. Lett. **53**, 2571 (1984); O. K. Andersen, O. Jepsen, and D. Gloetzel, in *Highlights of Condensed Matter Theory*, edited by F. Bassani, F. Fumi, and M. Tosi (North-Holland, Amsterdam, 1985).

[31] T. Bandyopadhyay and D. D. Sarma, Phys. Rev. B **39**, 3517 (1989).

[32] J. F. Janak, Phys. Rev. B **16**, 255 (1977).

[33] G. Fabricius, A. M. Llois, M. Weissmann, and M. A. Khan, Phys. Rev. B **49**, 2121 (1994).

[34] J. Guevara, F. Parisi, A. M. Llois, and M. Weissmann, Phys. Rev. B **55**, 13283 (1997); J. Guevara, A. M. Llois, and M. Weissmann, Phys. Rev. Lett. **81**, 5306 (1998).

[35] V. L. Moruzzi, J. F. Janak, and A. R. Williams, *Calculated Electronic Properties of Metals* (Pergamon, New York, 1978).

[36] J. W. Cable, Phys. Rev. B **15**, 3477 (1977).

[37] Y. Xie and J. A. Blackman, Phys. Status Solidi A **189**, 763 (2002).

[38] Y. C. Bae, V. Kumar, H. Osanai, and Y. Kawazoe, Phys. Rev. B **72**, 125427 (2005).

[39] C. Barreteau, R. Guirado-Lopez, D. Spanjaard, M. C. Desjonqueres, and A. M. Oles, Phys. Rev. B **61**, 7781 (2000).

[40] T. Sondón and J. Guevara, J. Magn. Magn. Mater. **272**, E1247 (2004).

[41] D. Zitoun, M. Respaud, M. C. Fromen, M. J. Casanove, P. Lecante, C. Amiens, and B. Chaudret, Phys. Rev. Lett. **89**, 037203 (2002); D. Zitoun, M. Respaud, M. C. Fromen, M. J. Casanove, P. Lecante, C. Amiens, and B. Chaudret, J. Magn. Magn. Mater. **272**, 1536 (2004).

[42] A. Diaz-Ortiz, F. Aguilera-Granja, K. Michaelian, E. O. Berlanga-Ramirez, J. M. Montejano-Carrizales, and A. Vega, Physica B **370**, 200 (2005); E. O. Berlanga-Ramirez, F. Aguilera-Granja, J. M. Montejano-Carrizales, A. Diaz-Ortiz, K. Michaelian, and A. Vega, Phys. Rev. B **70**, 014410 (2004); E. O. Berlanga-Ramirez, F. Aguilera-Granja, J. M. Montejano-Carrizales, A. Diaz-Ortiz, K. Michaelian, and A. Vega, Physica B **354**, 278 (2004); M. Muñoz-Navia, P. Villaseñor-Gonzalez, J. Dorantes-Davila, and G. M. Pastor, Comput. Mater. Sci. **35**, 302 (2006).